JOURNAL OF AIRCRAFT
Vol. 35, No. 1, January–February 1998

Roll–Yaw Control at High Angle of Attack by Forebody Tangential Blowing

Nelson Pedreiro*
EMBRAER, São José dos Campos 12225, Brazil
and
Stephen M. Rock,† Zeki Z. Celik,‡ and Leonard Roberts§
Stanford University, Stanford, California 94305-4035

The feasibility of using forebody tangential blowing as the only actuator to control the roll–yaw motion of a wind-tunnel model at high angles of attack is demonstrated experimentally. To accomplish this, a unique model is developed that describes the unsteady aerodynamic moments generated by both vehicle motion and the applied blowing. This model is sufficiently detailed to predict the transient motion of the wind-tunnel model, but is simple enough to be suitable for control design and implementation. Successful closed-loop control is demonstrated experimentally for a delta wing body model incorporating a 70-deg sweep angle and a cone–cylinder fuselage. Experiments were performed at 45-deg nominal angle of attack. At this condition, the natural motion of the system is divergent.

Nomenclature

b	=	wingspan
C_l	=	roll moment coefficient, $M_x/q_\infty S_{\text{ref}} b$
C_n	=	yaw moment coefficient, $M_z/q_\infty S_{\text{ref}} b$
C_μ	=	jet momentum coefficient, $\dot{m}_j V_j/q_\infty S_{\text{ref}}$
D	=	diameter of fuselage
I_A	=	inertia of support about γ axis
I_M	=	inertia of the wind-tunnel model in body frame
L	=	axial distance from tip of the forebody
M_z	=	yaw moment
M_γ	=	moment about γ axis
M_ϕ, M_x	=	moment about ϕ axis, roll moment
$\dot{m}_j$	=	jet mass flow rate
P	=	intersection of ϕ and γ axis
p, q, r	=	roll, pitch, and yaw rates, respectively
q_∞	=	dynamic pressure, $\rho U^2/2$
S_{ref}	=	reference area, wing planform area
U	=	freestream velocity
xyz	=	body-fixed reference frame, centered at P
γ	=	second degree of freedom
ρ	=	air density
ϕ	=	first degree of freedom, roll angle

I. Introduction

FLIGHT at high angles of attack allows for enhanced maneuverability and increased lift during takeoff and landing. At these flight conditions, the aerodynamics of the vehicle are dominated by separated flow, vortex shedding, and possibly vortex breakdown. These phenomena severely compromise the effectiveness of conventional control surfaces. Alternate means to control the vehicle at these flight regimes are therefore necessary, and several methods of altering the flow have been proposed to provide this increased control. As examples: nose bluntness and body trips have been shown to alleviate lateral loads,[1] deployable forebody strakes can be used to generate yaw moment,[2] and pneumatic actuators have been used as an effective means of altering the loads acting on the vehicle. In particular, Skow et al.[3] proposed the use of forebody vortex blowing to enhance departure characteristics of fighter aircraft, Wong et al.[4] demonstrated experimentally the use of leading-edge tangential blowing to suppress the roll oscillation of a delta wing, Alexan et al.[5] demonstrated a high-efficiency forebody blowing technique to generate side force and yaw moment on slender bodies, and Celik et al.[6–8] showed that forebody tangential blowing can be used to generate static aerodynamic loads.

The research reported here investigated the use of forebody tangential blowing (FTB) to augment the dynamic controllability of aircraft at high angles of attack. The method consists of injecting a thin sheet of air tangentially along the forebody of the vehicle. This causes changes in the forebody separation lines and, as a consequence, the strength and positions of the shed vortices are altered. These changes, introduced near the apex of the forebody, affect the flow over the entire length of the vehicle, and as a result the aerodynamic loads are modified. A feature of this approach is that large loads can be created using very small amounts of injected air. However, this relationship is highly nonlinear.

The effectiveness of using FTB to create aerodynamic loads has been well documented experimentally.[6–8] In particular, the generation of side force, roll, and yaw moments have been demonstrated for angles of attack from 20 to 50 deg. Most of this work has focused only on the measurement of static aerodynamic loads. Consequently, while these results have demonstrated the control authority of FTB, they have not demonstrated the ability of FTB to control the dynamic response of a vehicle, nor have they yielded a model of the phenomenon that is suitable for use in the development of a control law, i.e., inclusion of transient behavior.

Some work has focused on the use of forebody blowing as a dynamic actuation system in aircraft control laws, but most of this has been done only in simulation with approximate system models. For example, Adams et al.[9] investigated the use of forebody vortex blowing to expand the flight envelope of an F-16. They created nonlinear control laws based on a forebody blowing system that was assumed to function as an

Received Feb. 13, 1997; revision received Aug. 6, 1997; accepted for publication Aug. 7, 1997.

*Engineer; currently Ph.D. Candidate, Stanford University, Department of Aeronautics and Astronautics, Stanford, CA 94305-4035.

†Associate Professor, Department of Aeronautics and Astronautics. Senior Member AIAA.

‡Research Associate, Department of Aeronautics and Astronautics. Member AIAA.

§Emeriti Professor, Department of Aeronautics and Astronautics. Fellow AIAA.

incremental actuator, independent of the vehicle's attitude. Their simulation combined a high-fidelity F-16 model with static data on the effect of blowing on the roll and yaw moments. Adams et al.'s[9] results are significant in that they offer some insight into how control laws might be designed using this nonlinear phenomenon, and they predict significant potential performance improvements. However, even though the model used for the vehicle dynamics is complex and nonlinear, the blowing effect is incorporated based on several simplifying assumptions that are not supported experimentally.

In this paper, a mathematical model that describes both the static and transient characteristics of the aerodynamic loads created by forebody tangential blowing is generated and validated experimentally. This is done for a delta wing body combination that is installed in a low-speed wind tunnel. This vehicle is equipped with forebody slots, through which blowing is applied, and is constrained to move in two degrees of freedom: 1) rotation about the vehicle's longitudinal axis (roll), and 2) rotation about an axis normal to the roll axis (approximating yaw). It is shown that the effects of forebody tangential blowing on the roll and yaw moments in this system depend on the attitude of the vehicle, and that the stability derivatives of the vehicle depend on the amount of blowing applied. Consequently, FTB should not, in general, be treated as an incremental actuator. Further, the model of the unsteady aerodynamic loads developed here includes the effects of FTB and is of a form that is suitable for use in control law development. In particular, it is used in the design and real-time implementation of a control logic for the wind-tunnel system.

The paper is organized as follows, first, the experimental apparatus and its capabilities are described. This defines the scope and provides a context for all of the experimental results. Next, the equations of motion for the two-degrees-of-freedom apparatus are presented. This is followed by a set of flow visualization results that provides insight into the physics of the flow and forms the basis on which the transient aerodynamic model is then generated. Finally, a control approach is proposed and demonstrated that uses the developed aerodynamic model for the design and implementation of a closed-loop control logic that stabilizes the system.

II. Experimental Apparatus

A. Wind Tunnel and Model

The wind-tunnel facility used for these experiments consists of a closed-circuit low-speed wind tunnel with a 0.45 × 0.45 m test section. The maximum freestream airspeed in the test section is 60 m/s. The model installed in this tunnel consists of a sharp leading-edge symmetric delta wing with a 70-deg sweep angle and a cone–cylinder fuselage. The detailed geometry and inertia properties of the model are given in Ref. 10. A scale drawing of the model is shown in Fig. 1. Slots

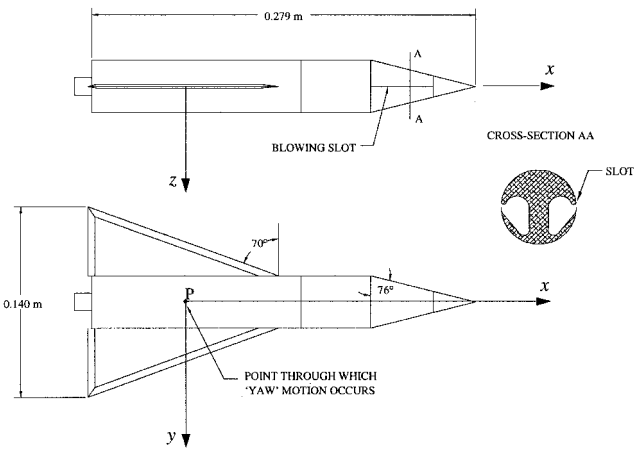

Fig. 1 Wind-tunnel model and detail of blowing slots.

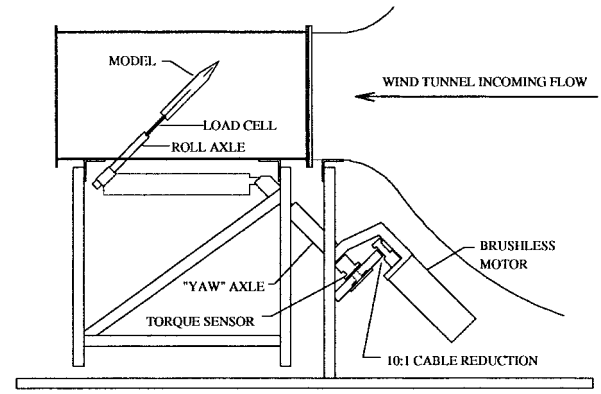

Fig. 2 Side view of test section and two-degrees-of-freedom model support system.

through which blowing is applied are present on both sides of the conical forebody. Air is provided to the forebody plena through flexible tubing that enters the model through the rear end of the fuselage. All tests were conducted at 19.5 m/s and a nominal angle of attack of 45 deg. For this condition, the Reynolds number based on the wing root chord is 2.6×10^5. Tunnel blockage at the nominal configuration is 7%. Figure 2 shows a side view of the test section with the model and the supporting mechanism.

B. Model Support System

A unique support system was designed and built that allows the model two degrees of freedom, which approximate the lateral–directional dynamics of an aircraft[10] (of particular interest is the roll–yaw coupling at high angle of attack). Two subsystems comprise the apparatus. The first implements the roll degree of freedom ϕ and consists of a shaft mounted on bearings. The wind-tunnel model is attached to this roll shaft and rotates freely about its longitudinal axis. This entire roll subsystem is then mounted on the second subsystem, which consists of a mechanical arm that can rotate about an axis perpendicular to the model's longitudinal axis (Fig. 2). This subsystem provides the second degree of freedom γ. $\dot{\phi}$ and $\dot{\gamma}$ are related to roll, pitch, and yaw rates (p, q, and r, respectively) as

$$p = \dot{\phi}, \qquad q = \dot{\gamma} \sin \phi, \qquad r = \dot{\gamma} \cos \phi \tag{1}$$

Mechanical constraints limit the degrees of freedom to $|\phi| < 105$ deg and $|\gamma| < 30$ deg. For convenience, the γ degree of freedom will be referred to as yaw, even though this is only an approximation, e.g., true for small ϕ.

Finally, this suspension is equipped with an active cancellation system that eliminates the inertia and gravity moment effects introduced into the system dynamics by the suspension system. This system consists of a brushless torque motor attached to the γ axle and a complement of sensors. In particular, two high-precision linear accelerometers are used to provide measurement of the angular acceleration $\ddot{\gamma}$, and a low-friction precision potentiometer provides a measurement of the angle γ. A specially designed torque sensor is also included. Measurements of γ and $\ddot{\gamma}$ are used in an outer control loop to calculate the effects of the suspension inertia and gravity restoring moment. The inverse of these moments is then issued as a command to the inner torque control loop. This combination provides sufficient bandwidth and accuracy for the cancellation logic. Experiments indicated that the friction in the bearings and the effect of the pressurized tubing are small in the roll degree of freedom when compared with the aerodynamic loads acting on the model,[7] and hence, did not need to be canceled.

C. Air Injection System

Air is injected independently through two slots located on either side of the conical portion of the forebody. The amount of air injected is controlled by a feedback system using specially designed flow meters and high bandwidth servovalves connected to a high-pressure supply. The amount of injected air is quantified by the jet momentum coefficient C_μ.

D. Instrumentation and Data Acquisition

In addition to the instrumentation mentioned in the preceding text, a low-friction precision potentiometer mounted to the ϕ axis is used to measure the roll angle, and a six-component force-torque sensor that connects the model to the roll shaft is used to provide both static and dynamic measurements of the aerodynamic loads.

For the flow visualization experiments, an argon–ion laser and an optical system are used to generate a laser sheet that is perpendicular to the model longitudinal axis. The optics are mounted on a traversing system located on top of the test section, allowing the laser sheet to be moved over the full length of the model. This capability is used in performing axial scans starting from the forebody and moving downstream to characterize the development of the flow structure. A smoke generator located upstream of the model is used to seed the flow. A video camera is located outside the test section aligned with the model longitudinal axis. The camera is used to record the results of the flow visualization and also the motion of the model during dynamic experiments.

Three microcomputers equipped with data acquisition boards are used in the experiments. One computer is dedicated to the active cancellation loop. A second computer is used to implement the closed-loop control of the vehicle, i.e., to control the amount of air injected in each plenum. A third computer is used for data acquisition.

III. Equations of Motion

The equations of motion of this system, including the effects of the suspension, can be expressed as

$$\begin{aligned} &I_{M_x}\ddot{\phi} + \sin\phi\cos\phi(I_{M_z} - I_{M_y})\dot{\gamma}^2 + \cos\phi I_{M_{xz}}\ddot{\gamma} = M_\phi \\ &(I_A + I_{M_y}\sin^2\phi + I_{M_z}\cos^2\phi)\ddot{\gamma} \\ &\quad + 2\cos\phi\sin\phi(I_{M_y} - I_{M_z})\dot{\phi}\dot{\gamma} \\ &\quad + (\ddot{\phi}\cos\phi - \dot{\phi}^2\sin\phi)I_{M_{xz}} = M_\gamma \end{aligned} \tag{2}$$

For the current model configuration, where a vertical stabilizer is not present, the product of inertia $I_{M_{xz}}$ is zero.

In these equations, M_ϕ represents the total moment applied about the longitudinal axis of the model, and M_γ represents the moment about the γ axis.

M_ϕ and M_γ are given by

$$\begin{aligned} M_\phi &= M_\phi^A + M_\phi^T + M_\phi^F \\ M_\gamma &= M_\gamma^A + M_\gamma^T + M_\gamma^F + M_\gamma^G + M_\gamma^M \end{aligned} \tag{3}$$

where the superscripts indicate the origin of the moments: A is for aerodynamics, T is for air supply tubing, F is for friction, G is for gravity, and M is for motor. For $|\phi| < 40$ deg, the moment caused by the air supply tubing about the ϕ axis, M_ϕ^T, was found to be negligible.

The effects of the suspension inertia, the gravity restoring moment, and the restoring moment as a result of the tubing (in the yaw degree of freedom) are represented by the terms $I_A\ddot{\gamma}$, $-k_G\sin\gamma$, and $-k_T\gamma$, respectively. These can be canceled by the active cancellation system by specifying the moment applied by the torque motor to be

$$M_\gamma^M = I_A\ddot{\gamma}_m + k_G\sin\gamma_m + k_T\gamma_m \tag{4}$$

where the subscript m indicates measured values of the quantities, and the coefficients are constants determined experimentally.

The moments caused by friction of the bearings and potentiometers can be written as

$$M_\phi^F = -C_F\dot{\phi}, \qquad M_\gamma^F = -D_F\dot{\gamma} \tag{5}$$

where C_F and D_F were determined experimentally.

Substituting expressions (4) and (5) in Eq. (3), and using the approximation sign to indicate that the cancellation is not perfect,[10,11] yields

$$\begin{aligned} M_\phi &\approx M_\phi^A - C_F\dot{\phi} \\ M_\gamma &\approx M_\gamma^A - D_F\dot{\gamma} + I_A\ddot{\gamma} \end{aligned} \tag{6}$$

Expressions for the aerodynamic moments M_ϕ^A and M_γ^A are necessary to complete Eq. (6). In the following section, experimental results are presented that characterize the nature of the aerodynamic phenomena to be modeled. This is followed by the formulation of a model that successfully calculates the unsteady aerodynamic loads acting on the vehicle.

IV. Aerodynamics

A. Flow Visualization

Figure 3 presents the results of some experiments that reveal the basic structure of the flow. Although four main vortices were expected, two from the forebody and two from the wing leading edges, experiments demonstrated that, in general, only three separate vortical structures can be clearly identified, even for a symmetric condition in which $\phi = \gamma = 0$, and no blowing is applied (Fig. 3b). By performing axial scans with the laser sheet, it was observed that the asymmetry starts early on the forebody, i.e., close to the tip of the cone, and scales up over the entire forebody.[11] As a result of the asymmetry, one vortex will be close to the fuselage and the other will be displaced and be further away (Fig. 3a). For the sections where the wing

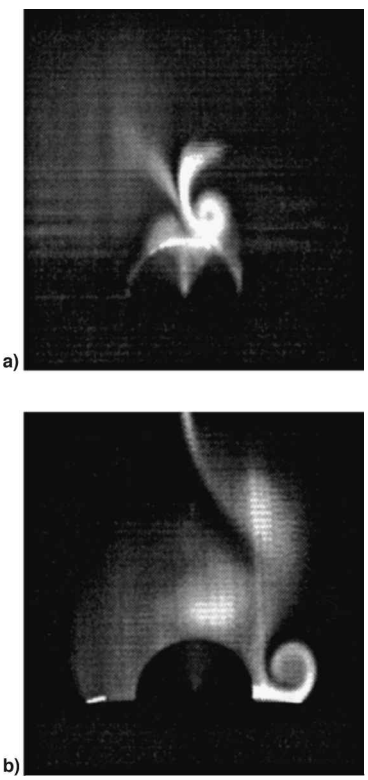

Fig. 3 Smoke flow visualization results. $\phi = \gamma = 0$, no blowing is applied. a) Station 1, forebody, $L/D = 3$; and b) station 2, wing–body, $L/D = 5$.

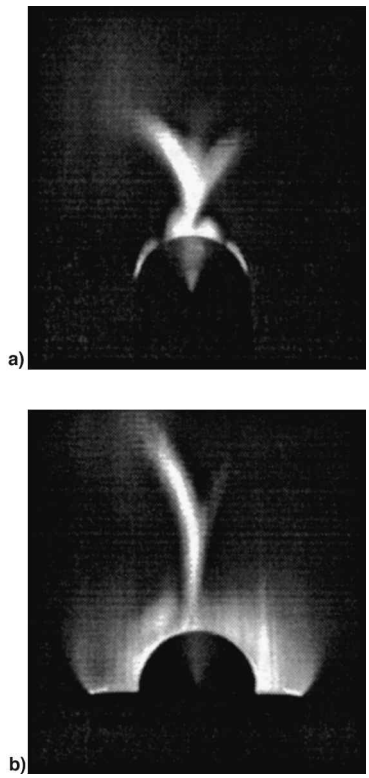

Fig. 4 Smoke flow visualization results. Symmetric blowing, $\phi = \gamma = 0$, $C_\mu = 0.0075$. a) Station 1, forebody, $L/D = 3$; and b) station 2, wing–body, $L/D = 5$.

is present, it was observed that a vortex is formed close to the wing on the same side where the forebody vortex is far from the fuselage. For the side where the forebody vortex is close to the fuselage, no wing vortex is clearly identified.

The effect of asymmetric blowing, i.e., blowing applied from one side only, is mainly to increase the asymmetry or invert it, depending on which side the blowing is applied from. Blowing moves the separation lines on the forebody and changes the amount of vorticity that is shed. As a consequence, the strength and positions of the vortices are affected by blowing. Experiments have shown that there is a finite amount of blowing that needs to be applied to invert the asymmetry of the flow. For the current model configuration at $\phi = \gamma = 0$, this value is $C_\mu \approx 0.0045$.

The application of symmetric blowing has the effect of changing the flow structure to a more symmetric one (Fig. 4). For high values of symmetric blowing, the flow can be considered attached on the forebody and its structure is very symmetric along the whole length of the model.

Experiments showed that the asymmetric structure can change significantly by a change in the roll angle. The flow structure is not as sensitive to a change in γ.

B. Static Aerodynamic Loads

Static measurements for the roll and yaw moment as a function of ϕ, γ, and C_μ are presented in Figs. 5–7, respectively, for a nominal angle of attack of 45 deg. The accuracy of the measurements of C_l and C_n are, respectively, ± 0.0025 and ± 0.016. A convention is adopted that right side, i.e., starboard, blowing is positive and left side, i.e., port side, blowing is negative. In Fig. 5, the effect of the roll angle on C_l and C_n is shown for $\gamma = 0$ and various C_μ. The C_l curve for $C_\mu = 0$ presents a change in slope for $\phi \approx -15$ deg. For $C_\mu = 0.02$,

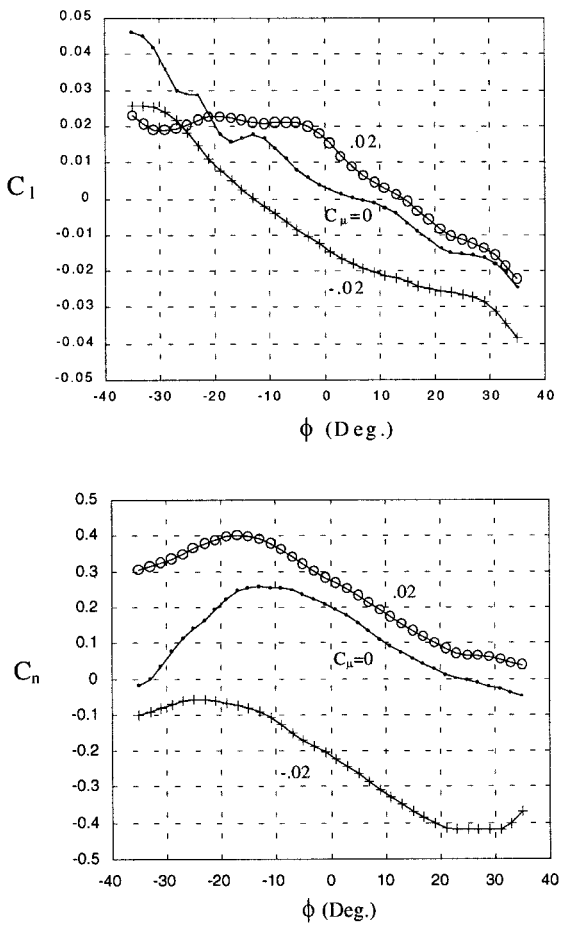

Fig. 5 Roll angle effect on roll and yaw moment coefficients C_l and C_n, for $\gamma = 0$.

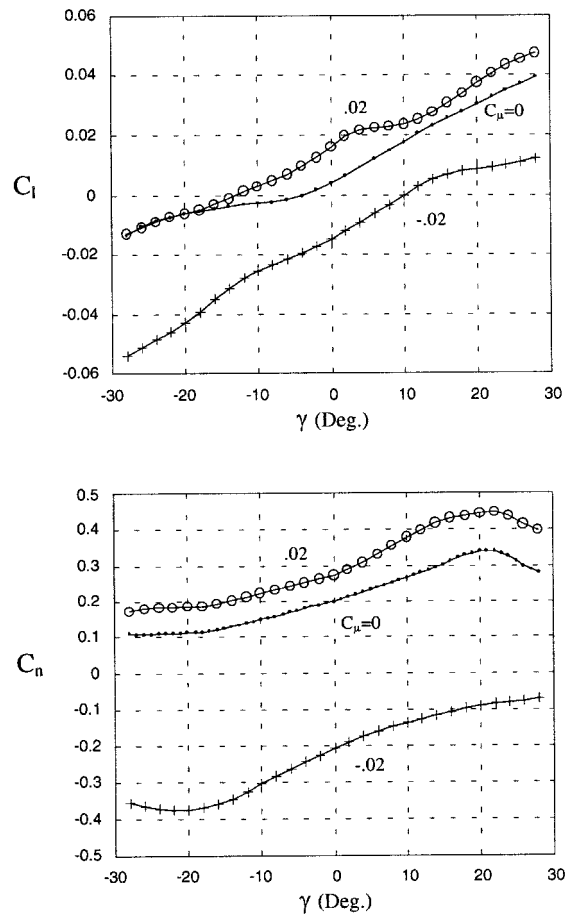

Fig. 6 Effect of γ angle on roll and yaw moment coefficients C_l and C_n, for $\phi = 0$.

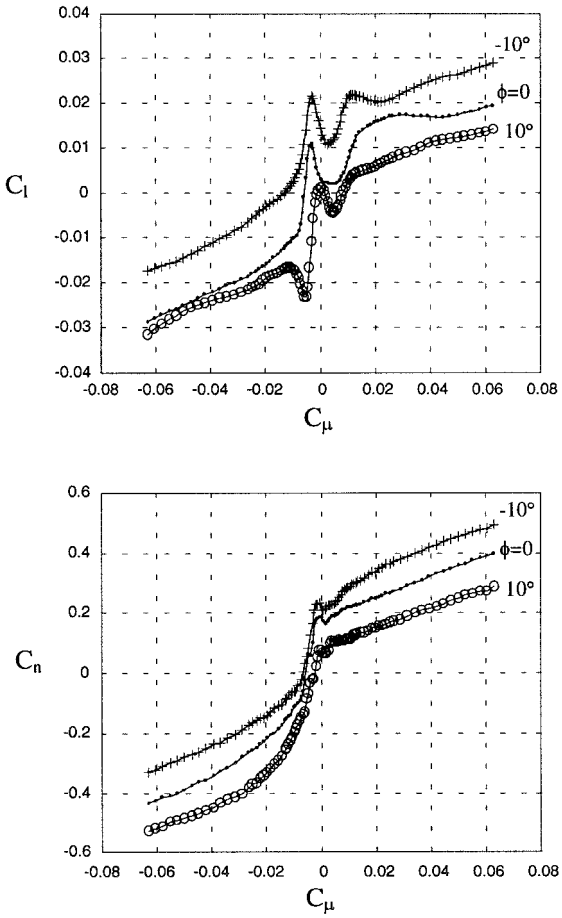

Fig. 7 Effect of asymmetric blowing on roll and yaw moment coefficients C_l and C_n, for $\gamma = 0$.

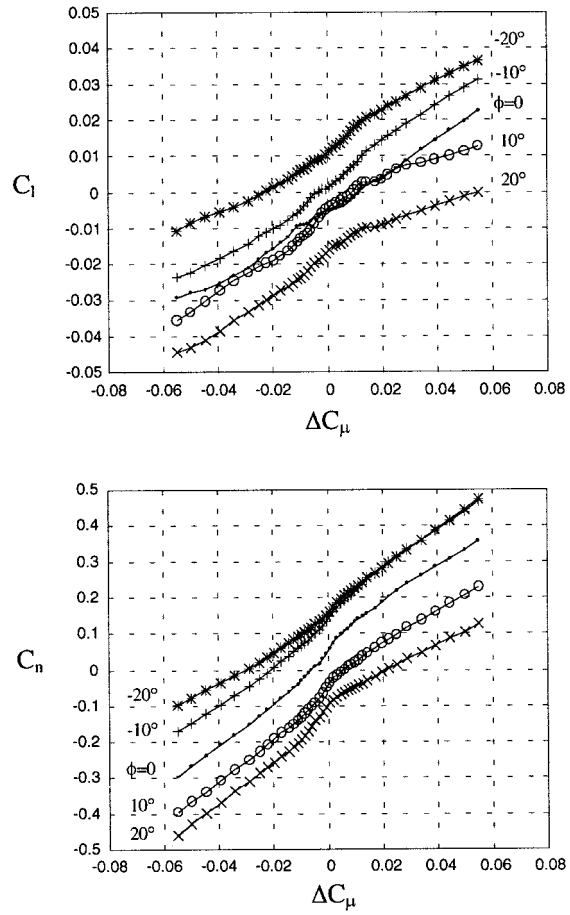

Fig. 8 Effect of symmetric plus asymmetric blowing on roll and yaw moment coefficients for $C_{\mu_{SYM}} = 0.01$ and $\gamma = 0$.

a change occurs at $\phi \approx -5$ deg. Also for $C_\mu = 0$, the C_n curve presents a large change in slope for $\phi < -15$ deg. The fact that these changes are not symmetric, i.e., they only occur for $\phi < 0$, indicates that they are caused by geometrical imperfections on the tip of the conical forebody. The slopes of the curves represent the stability derivatives in ϕ and γ, and it is clearly seen in the plots that those are dependent on the amount of blowing applied.

Figure 6 presents curves for C_l and C_n vs γ for $\phi = 0$ and various C_μ. Comparing Figs. 5 and 6 shows that the slopes of the roll and yaw moment curves are not as sensitive to γ as they are to ϕ. This is in agreement with the flow visualization experiments that indicated the flow structure to be less dependent on γ than on ϕ. The effect of asymmetric blowing on C_l and C_n is shown in Fig. 7 for $\gamma = 0$ and various ϕ. In this case, blowing is applied either on the right or left side. As seen, the roll moment varies abruptly for $|C_\mu| < 0.01$, and the yaw moment presents a large variation for $-0.01 < C_\mu < 0$. The roll and yaw moments generated by blowing are functions of the attitude of the vehicle, particularly in the region where the values of C_μ are small. Degani[12] showed that small amounts of blowing have an effect similar to the geometric imperfections near the tip of the forebody and can cause flow instabilities that lead to asymmetry in the flow. This is the most plausible explanation for the roll moment behavior shown in Fig. 7.

Figure 8 shows the result of applying symmetric and incremental asymmetric blowing on the roll and yaw moment coefficients. An equal amount of blowing, $C_{\mu_{SYM}}$, is applied on both sides, and additional asymmetric blowing, ΔC_μ, is applied either to the right or left side. As seen, the major effect is to produce a linear characteristic that eliminates the sudden variations that occur in the asymmetric blowing case. The symmetry observed in these plots agrees with the symmetric flow

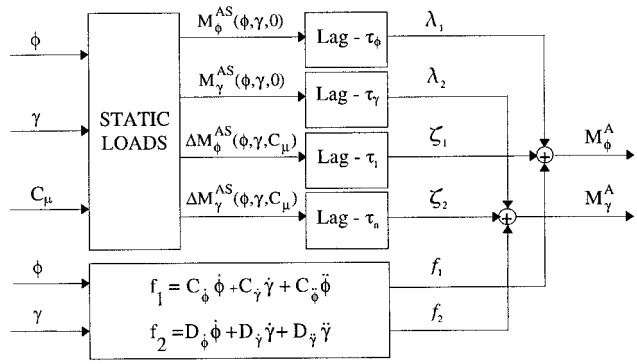

Fig. 9 Structure of the aerodynamic model. M_ϕ^{AS} and M_γ^{AS} represent static roll and yaw moments, respectively.

structure obtained from the flow visualization experiments (Fig. 4).

V. Transient Aerodynamic Model

The preceding data define the steady-state components of the aerodynamic moments M_ϕ^A and M_γ^A as functions of the model degrees of freedom ϕ and γ and the injected airflow C_μ. A complete description of these moments, i.e., sufficiently detailed for use in the development of dynamic control algorithms, requires the inclusion of the transient effects as well.

The procedure incorporated here for developing this transient model involved hypothesizing a model structure based on observations made during the flow visualization studies, and then fitting the unknown parameters in this model using measured transient data and well-known parameter identifica-

tion procedures. The utility of the resulting model is validated by its ability to predict and match experimental measurements.

The model form that was hypothesized is shown in Fig. 9. Inputs to this model are the two degrees of freedom ϕ and γ and the amount of blowing C_μ. The outputs are the unsteady roll and yaw moments M_ϕ^A and M_γ^A. This model is an extension of the model used successfully by Wong et al.[4] for a delta wing undergoing roll oscillations. The static aerodynamic loads determined earlier are an integral part of this model. Also note that the difficult-to-model effects of the conical forebody can be included conveniently here as part of the tabulated steady-state data.

The transient characteristics included in this structure are of two basic types. First are the effects associated with the motion of the vehicle. These include aerodynamic damping, roll–yaw cross-coupling, and the apparent mass of the fluid. They are modeled as

$$f_1 = C_{\dot\phi}\dot\phi + C_{\dot\gamma}\dot\gamma + C_{\ddot\phi}\ddot\phi$$
$$f_2 = D_{\dot\phi}\dot\phi + D_{\dot\gamma}\dot\gamma + D_{\ddot\gamma}\ddot\gamma \tag{7}$$

where the coefficients of $\dot\phi$, $\dot\gamma$, $\ddot\phi$, and $\ddot\gamma$ are constants determined experimentally.

Second, it is assumed that there are characteristic times associated with the flow being able to reorganize itself as a result of either a change in vehicle attitude or a change in the applied level of blowing. These effects are included by lagging the static loads. Research on the nonlinear aerodynamic response to vehicle motion has indicated that the characteristic times associated with vortex breakdown are considerably larger than the convection time, and that the aerodynamic loads may depend on the past time history of vehicle motion.[13–16] Incorporating all of these effects results in a complex aerodynamic model that is not suitable for control logic design and real-time implementation. Instead, a simplified model is used here incorporating first-order time constants τ_ϕ and τ_γ to represent a lag in the static loads caused by the motion of the vehicle only. This form was determined by comparing static and dynamic flow visualization results, which clearly show that the dynamic positions of the vortices lag with respect to the static ones.[8] The current approach lumps position and strength effects by lagging the loads to represent their combined effect. Time constants τ_l and τ_n account for the fact that blowing is applied at the forebody and convection is necessary for sections of the vehicle further downstream to be affected.

Given the structure shown in Fig. 9 and the expressions for f_1 and f_2, the equations for the aerodynamic moments M_ϕ^A and M_γ^A are

$$M_\phi^A = \lambda_1 + \zeta_1 + C_{\dot\phi}\dot\phi + C_{\dot\gamma}\dot\gamma + C_{\ddot\phi}\ddot\phi$$
$$M_\gamma^A = \lambda_2 + \zeta_2 + D_{\dot\phi}\dot\phi + D_{\dot\gamma}\dot\gamma + D_{\ddot\gamma}\ddot\gamma \tag{8}$$

λ_1 and λ_2 are the lagged static roll and yaw moments for $C_\mu = 0$, respectively, and are given by

$$\tau_\phi\dot\lambda_1 + \lambda_1 = M_\phi^{AS}$$
$$\tau_\gamma\dot\lambda_2 + \lambda_2 = M_\gamma^{AS} \tag{9}$$

ζ_1 and ζ_2 represent the effects of blowing on the roll and yaw moment and are given by

$$\tau_l\dot\zeta_1 + \zeta_1 = F_1(C_\mu)$$
$$\tau_n\dot\zeta_2 + \zeta_2 = F_2(C_\mu) \tag{10}$$

where τ_l and τ_n are time constants that characterize the roll and yaw moment response to a variation in blowing, ΔC_μ. They include the effect of valve and plenum dynamics as well as the time it takes for the change in the flow structure to affect the moments.

Figure 10 shows the response of C_l and C_n for a step input command in C_μ. Also shown are the results of the parameter fitting using Eqs. (10). The simplified model well represents the yaw moment response, but does not capture completely the high-frequency component of the roll moment transient response. This indicates that the assumed model is too simple to represent completely the complex physical phenomena that

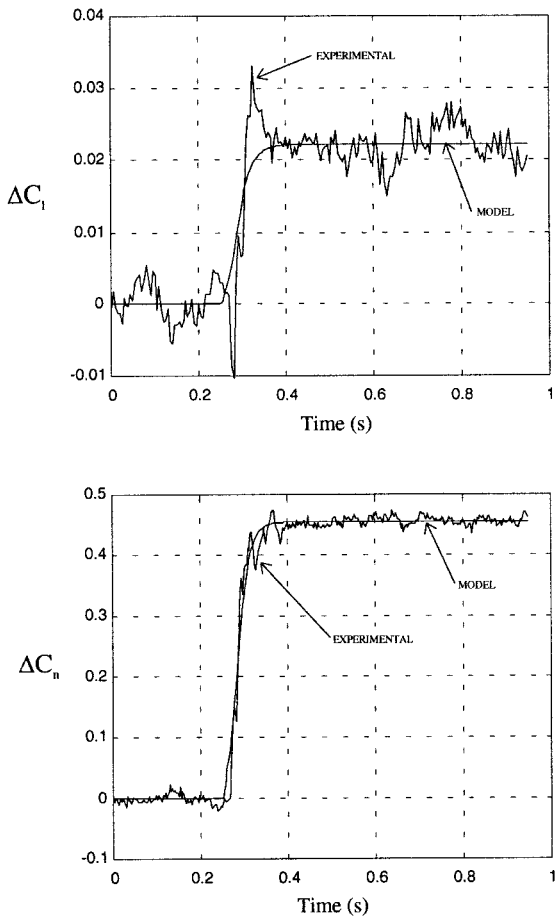

Fig. 10 C_l and C_n response to step input command in C_μ. ΔC_l and ΔC_n are used to indicate variation from the initial value.

Table 1 Identified parameters for the aerodynamic model and characteristics of the system

Parameter	Converged value ± σ
τ_ϕ	0.035 ± 0.006 s
τ_γ	0.023 ± 0.007 s
$C_{\dot\phi}$	$(-0.44 \pm 0.34) \times 10^{-3}$ nm s
$C_{\dot\gamma}$	$(-1.02 \pm 0.02) \times 10^{-3}$ nm s
$C_{\ddot\phi}$	$(0.4 \pm 0.1) \times 10^{-4}$ nm s^2
$D_{\dot\phi}$	$(1.03 \pm 0.7) \times 10^{-3}$ nm s
$D_{\dot\gamma}$	$(-2.5 \pm 0.7) \times 10^{-3}$ nm s
$D_{\ddot\gamma}$	$(-1.18 \pm 1.0) \times 10^{-3}$ nm s^2
τ_l	0.040 ± 0.001 s
τ_n	0.023 ± 0.001 s
I_{M_x}	$(2.60 \pm 0.20) \times 10^{-4}$ kg m^2
I_{M_y}	$(3.19 \pm 0.05) \times 10^{-3}$ kg m^2
I_{M_z}	$(3.22 \pm 0.02) \times 10^{-3}$ kg m^2
$I_{M_{yz}}$	≈0 kg m^2
I_A	0.159 ± 0.001 kg m^2
k_T	≈0 nm
k_G	3.305 ± 0.033 nm
C_F	$(1.1 \pm 0.3) \times 10^{-3}$ nm s
D_F	$(8.5 \pm 2.6) \times 10^{-3}$ nm s

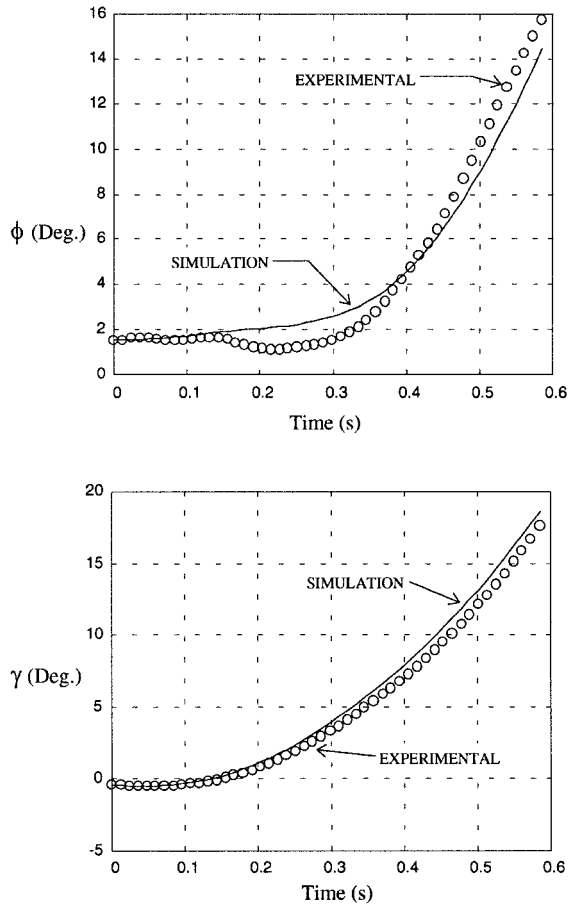

Fig. 11 Natural motion of the two-degrees-of-freedom system, experiment and simulation.

take place when blowing is applied. However, the ability of this model to predict overall vehicle motion suggests that it is sufficiently accurate for the current studies.

Substituting Eqs. (6–10) into Eq. (2), the equations of motion for the two-degrees-of-freedom system are obtained. Dynamic stability derivatives and time constants τ_ϕ and τ_γ are determined using a least-squares fit to the time histories of ϕ and γ for a set of dynamic experiments. Time constants τ_l and τ_n are determined from the roll and yaw moment response to a step input command in C_μ (Fig. 10). Table 1 contains the values identified for the various coefficients and the associated standard deviation. Also included are the values for the parameters that characterize the two-degrees-of-freedom system. The large standard deviation of some of the values reflects the approximation entailed in this lumped-parameter model.

The natural motion of the system is shown in Fig. 11 for the case where the model is released from $\phi \approx \gamma \approx 0$. Blowing is not applied during this experiment. Experimental results are compared with simulation using the aerodynamic model developed. The simulation agrees well with the measured response.

As seen from the time histories of ϕ and γ, the system is unstable. The natural motion is divergent and is stopped when the system approaches the mechanical limit of γ. The need for control is demonstrated and a control approach that stabilizes the system using blowing as the only actuator is discussed next.

VI. Closed-Loop Control

To design a control law that stabilizes the naturally unstable system, the equations of motion are linearized as follows. For small variations about the static equilibrium roll and yaw angles ϕ_E and γ_E, ϕ and γ are redefined as $\phi - \phi_E$ and $\gamma - \gamma_E$,

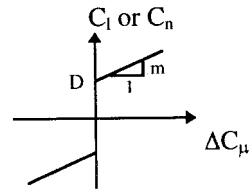

Fig. 12 Characteristic of C_l and C_n vs ΔC_μ.

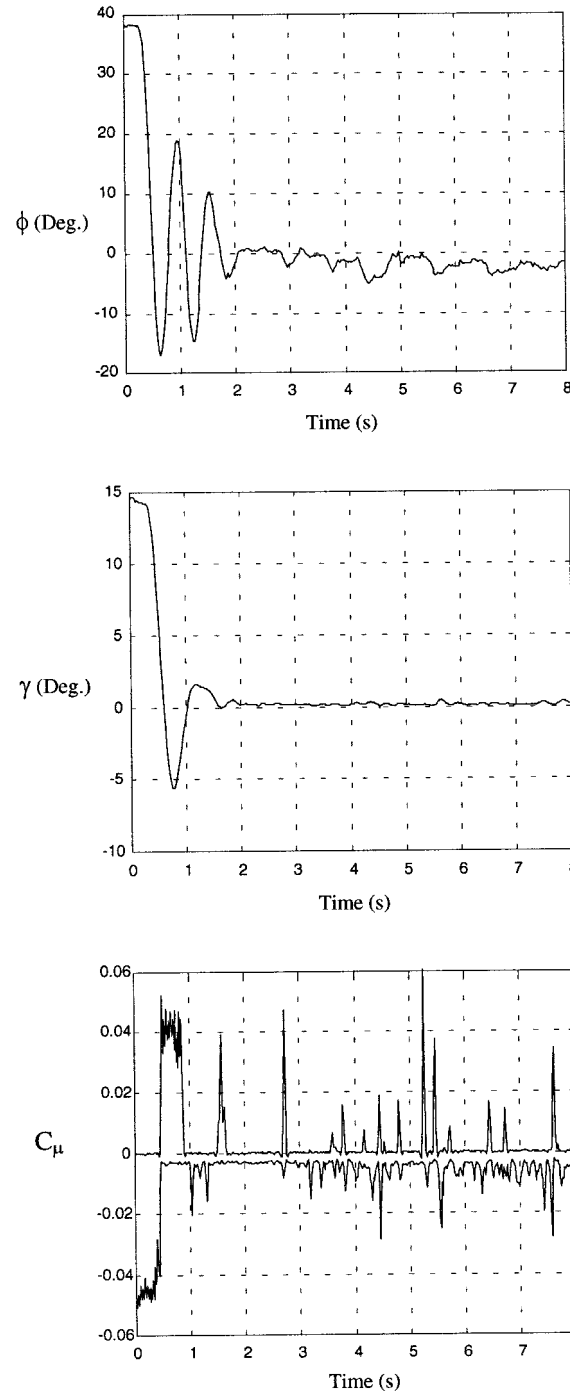

Fig. 13 Closed-loop control of the two-degrees-of-freedom system, response to initial condition, asymmetric blowing $C_{\mu 0} = 0.01$.

respectively, and for the current case where $I_{M_{xz}} \approx 0$ and ϕ_E and γ_E are small, Eqs. (2) and (6) are written as

$$I_{M_x}\ddot{\phi} + C_F\dot{\phi} = M_\phi^A$$
$$I_{M_z}\ddot{\gamma} + D_F\gamma = M_\gamma^A \tag{11}$$

About the static equilibrium position, M_ϕ^{AS} and M_γ^{AS} can be expressed as

$$M_\phi^{AS} = C_\phi \phi + C_\gamma \gamma$$
$$M_\gamma^{AS} = D_\phi \phi + D_\gamma \gamma \tag{12}$$

where C_ϕ, C_γ, D_ϕ, and D_γ are the static stability derivatives obtained from the curves for the roll and yaw moments vs ϕ and γ. Numerical values for these quantities are given in Table 2.

Equations (10) represent the effect of blowing, which is, in general, nonlinear as determined by functions F_1 and F_2. Investigation of different blowing techniques indicates how a linearized description of the blowing effect can be obtained.

First consider the case where only asymmetric blowing is applied. In this case, and for $|C_\mu| < 0.01$, F_1 and F_2 are highly nonlinear functions of C_μ, as seen in Fig. 7. Furthermore, operation in this region is prone to generating nonrobust control laws because C_l and C_n are very sensitive to small variations in blowing. Given these reasons, the low blowing intensities are avoided by employing the following control strategy. A minimum amount of asymmetric blowing other than zero $C_{\mu 0}$ is chosen, and additional blowing ΔC_μ is added to that value, i.e.,

$$C_\mu \equiv C_{\mu 0} + \Delta C_\mu \tag{13}$$

The curves for C_l and C_n vs ΔC_μ have the general form shown in Fig. 12.

A describing function approach is used to determine the equivalent gain of curves C_l and C_n vs ΔC_μ. The actual gain, $N(A)$, depends on the amplitude of the input A, and is given by

$$N(A) = (4D/\pi A) + m \tag{14}$$

D and m are defined in Fig. 12. An average amplitude is selected for ΔC_μ and used to calculate C_B and D_B, the equivalent gains for roll and yaw moment, respectively (Table 2). The resulting expressions for F_1 and F_2 are

$$F_1 = C_B \Delta C_\mu, \qquad F_2 = D_B \Delta C_\mu \tag{15}$$

A second approach consists of superimposing symmetric plus asymmetric blowing. In this case, the use of the describing function is dispensed because the C_l and C_n dependence on ΔC_μ is fairly linear (Fig. 9), i.e., functions F_1 and F_2 have the form shown in Eqs. (15).

The first approach, i.e., use of asymmetric blowing only, is chosen here because it uses less air than the approach of combined symmetric plus asymmetric blowing.

The linearized equations of motion are

$$\begin{aligned}
(I_{M_{\dot{x}}} - C_{\dot{\phi}})\ddot{\phi} &= (C_{\dot{\phi}} - C_F)\dot{\phi} + C_\gamma \dot{\gamma} + \lambda_1 + \zeta_1 \\
(I_{M_{\dot{z}}} - D_{\dot{\gamma}})\ddot{\gamma} &= (D_{\dot{\gamma}} - D_F)\dot{\gamma} + D_\phi \dot{\phi} + \lambda_2 + \zeta_2 \\
\tau_\phi \dot{\lambda}_1 + \lambda_1 &= C_\phi \phi + C_\gamma \gamma \\
\tau_\gamma \dot{\lambda}_2 + \lambda_2 &= D_\phi \phi + D_\gamma \gamma \\
\tau_l \dot{\zeta}_1 + \zeta_1 &= C_B \Delta C_\mu \\
\tau_n \dot{\zeta}_2 + \zeta_2 &= D_B \Delta C_\mu
\end{aligned} \tag{16}$$

which can be written in the form

$$\dot{\boldsymbol{x}}(t) = A\boldsymbol{x}(t) + Bu(t) \tag{17}$$

where $\boldsymbol{x}$ is the state vector and u the control variable

$$\boldsymbol{x} \equiv [\dot{\phi}\ \dot{\gamma}\ \phi\ \gamma\ \lambda_1\ \lambda_2\ \zeta_1\ \zeta_2]^T, \qquad u \equiv \Delta C_\mu \tag{18}$$

The resulting A and B matrices are given by

$$A = \begin{bmatrix}
-7.0 & -4.64 & 0 & 0 & 4545.45 & 0 & 4545.45 & 0 \\
0.24 & -2.51 & 0 & 0 & 0 & 228.31 & 0 & 228.31 \\
1 & 0 & 0 & 0 & 0 & 0 & 0 & 0 \\
0 & 1 & 0 & 0 & 0 & 0 & 0 & 0 \\
0 & 0 & -0.71 & 0.63 & -28.57 & 0 & 0 & 0 \\
0 & 0 & -6.22 & 6.22 & 0 & -43.48 & 0 & 0 \\
0 & 0 & 0 & 0 & 0 & 0 & -25.00 & 0 \\
0 & 0 & 0 & 0 & 0 & 0 & 0 & -43.48
\end{bmatrix} \tag{19}$$

$$B = [0\ 0\ 0\ 0\ 0\ 0\ 7.0\ 220.0]^T \tag{20}$$

Using this model, a controller was designed using the linear quadratic regulator (LQR) method with weights on $\dot{\phi}$, $\dot{\gamma}$, ϕ, γ, and ΔC_μ. The result is control of the form

$$u(t) = -\boldsymbol{K}\boldsymbol{x}(t) \tag{21}$$

where

$$\boldsymbol{K} = [0.00102\ \ 0.03198\ \ 0.00271\ \ 0.25156\ \ -0.29918\ \ 0.11332\ \ -0.29918\ \ 0.11332] \tag{22}$$

This control law requires knowledge of the state vector. ϕ and γ are measured directly. The other state variables are estimated from these measurements, and Eqs. (16), i.e., the linearized aerodynamic model, are used to reconstruct the state vector.

The performance of the closed-loop system is shown in Fig. 13. The plots show data obtained during a real-time closed-loop control experiment. In this case, the model was released from $\phi \approx 38$ deg and $\gamma \approx 14$ deg. It is seen that the logic makes the system stable and regulates ϕ and γ close to zero. The third plot shows the control effort C_μ. Two curves are shown: $C_\mu > 0$ for right-side blowing, and $C_\mu < 0$ for left-side blowing. The mean value of C_μ is less than 0.005 and gives a measure of the required average air mass flow rate. This value is within the capabilities of current fighter aircraft if the air is bled from the engines.[17] Larger values of C_μ (0.062 peak) are observed, but are applied over very short time intervals.

Table 2 Values for the static stability derivatives and linearized actuator gains

Parameter	Value
C_ϕ	−0.025 nm/rad
C_γ	0.022 nm/rad
D_ϕ	−0.143 nm/rad
D_γ	0.143 nm/rad
C_{μ_0}	0.01
C_B	0.28 nm
D_B	5.05 nm

Similar results are obtained using the second control approach, i.e., symmetric and asymmetric blowing. The disadvantage of this approach is a larger use of air when compared to the case where only asymmetric blowing is applied.

VII. Summary and Conclusions

The feasibility of using forebody tangential blowing (FTB) as the only actuator to stabilize the roll–yaw motion of a delta wing body model has been demonstrated experimentally in the wind tunnel. This result is the first to merge a validated unsteady aerodynamic model with an experimental demonstration of its utility in designing and implementing transient control laws. Similar results are expected for large Reynolds numbers because the technique used consists of generating aerodynamic loads by changing the separation lines on the forebody.

Further, a technique for developing an unsteady aerodynamic model that includes the effects of forebody tangential blowing and is suitable for controls is presented and validated. This model is based on a combination of static measurements of the aerodynamic loads with a lumped-parameter model that describes the main dynamic effects observed in flow visualization studies. The model is validated through dynamic experiments and is also used in the design and real-time implementation of closed-loop control laws.

The apparatus used in these experiments consists of a wing–body combination that is constrained to move in two degrees of freedom by a unique suspension system. The two degrees of freedom are an approximation to roll and yaw. Experiments were conducted at 45-deg nominal angle of attack and showed that the natural motion of the system is unstable exhibiting a divergent motion.

Flow visualization experiments indicated that the flow structure over the wing–body combination at 45-deg angle of attack is asymmetric. Also, the coupling between forebody vortices and wing vortices is strong, and an asymmetry that starts on the forebody will determine the structure of the flow downstream. At sections where the wing is present, three main vortical structures are discernible. It is shown that asymmetric blowing is a highly nonlinear effector that can be linearized by superimposing symmetric blowing. Asymmetric FTB increases the flow asymmetry or inverts it, depending on which side of the model blowing is applied from. The asymmetry can also be inverted by a change in roll angle. The flow structure is not as sensitive to changes in yaw angle. The transient response of roll and yaw moments to a step input blowing are determined.

Acknowledgments

This work was supported by the NASA–Stanford Joint Institute for Aeronautics and Acoustics, NASA Grant NCC 2-55, and the Air Force Office of Scientific Research, Grant F49620-96-1-0248. The first author was also supported by CNPq, Brazil, during the research for this paper.

References

[1]Ericsson, L. E., and Reding, J. P., "Alleviation of Vortex Induced Asymmetric Loads," *Journal of Spacecraft and Rockets*, Vol 17, No. 6, 1980, pp. 546–553.

[2]Rao, D. M., Moskovitz, C., and Murri, D. G., "Forebody Vortex Management for Yaw Control at High Angles of Attack," *Journal of Aircraft*, Vol. 24, No. 4, 1987, pp. 248–254.

[3]Skow, A. M., Moore, W. A., and Lorincz, D. J., *Forebody Vortex Blowing—A Novel Control Concept to Enhance Departure/Spin Recovery Characteristics of Fighter and Trainer Aircraft*, CP-262, AGARD, No. 24, 1979, pp. 24-1–24-17.

[4]Wong, G. S., Rock, S. M., Wood, N. J., and Roberts, L., "Active Control of Wing Rock Using Tangential Leading-Edge Blowing," *Journal of Aircraft*, Vol. 31, No. 3, 1994, pp. 659–665.

[5]Alexan, K., Hanff, E. S., and Kind, R. J., "Water-Tunnel Investigation of Dynamic Manipulation of Forebody Vortices," AIAA Paper 94-0503, Jan. 1994.

[6]Celik, Z. Z., and Roberts, L., "Vortical Flow Control on a Wing-Body Combination Using Tangential Blowing," AIAA Paper 92-4430, Aug. 1992.

[7]Celik, Z. Z., Roberts, L., and Pedreiro, N., "The Control of Wing Rock by Forebody Blowing," AIAA Paper 93-3685, Aug. 1993.

[8]Celik, Z. Z., Roberts, L., and Pedreiro, N., "Dynamic Roll and Yaw Control by Tangential Forebody Blowing," AIAA Paper 94-1853, June 1994.

[9]Adams, R. J., Buffington, J. M., and Banda, S. S., "Active Vortex Flow Control for VISTA F-16 Envelope Expansion," AIAA Paper 94-3681, Aug. 1994.

[10]Pedreiro, N., "Development of an Apparatus for Wind Tunnel Dynamic Experiments at High-α," NASA Joint Inst. for Aeronautics and Acoustics, TR-119, Stanford Univ., Stanford, CA, Feb. 1997.

[11]Pedreiro, N., "Experiments in Aircraft Roll-Yaw Control Using Forebody Tangential Blowing," Ph.D. Dissertation, Aeronautics and Astronautics Dept., Stanford Univ., Stanford, CA, 1997.

[12]Degani, D., "Numerical Investigation of the Origin of Vortex Asymmetry," AIAA Paper 90-0593, Jan. 1990.

[13]Grismer, D. S., and Jenkins, J. E., "Critical-State Transients for a Rolling 65-Degree Delta Wing," *Journal of Aircraft*, Vol. 34, No. 3, 1997, pp. 380–386.

[14]Jenkins, J. E., Myatt, J. H., and Hanff, E. S., "Body-Axis Rolling Motion Critical States of a 65-Degree Delta Wing," *Journal of Aircraft*, Vol. 33, No. 2, 1996, pp. 268–278.

[15]Ericsson, L. E., and Hanff, E. S., "Further Analysis of High-Rate Rolling Experiments of a 65-Degree Delta Wing," *Journal of Aircraft*, Vol. 31, No. 6, 1994, pp. 1350–1357.

[16]Tobak, M., and Chapman, G. T., "Nonlinear Problems in Flight Dynamics Involving Aerodynamic Bifurcations," *AGARD Symposium on Unsteady Aerodynamics—Fundamentals and Applications to Aircraft Dynamics*, CP-386, AGARD, 1985, pp. 25-1–25-15.

[17]Kroo, I., and Roberts, L., "Forebody Tangential Blowing for Control at High Angles of Attack—Feasibility Study Final Report," NASA Joint Inst. for Aeronautics and Acoustics, TR-101, Stanford Univ., Stanford, CA, June 1991.